Hyaluronic Acid—Quantum Dot Conjugates for *In Vivo* Lymphatic Vessel Imaging

Suk Ho Bhang,[¶,†] Nayoun Won,[¶,‡] Tae-Jin Lee,[†] Ho Jin,[‡] Jutaek Nam,[‡] Joonhyuck Park,[‡] Hyokyun Chung,[‡] Hyun-Seo Park,[§] Yung-Eun Sung,[§] Sei Kwang Hahn,[∥] Byung-Soo Kim,[†,*] and Sungjee Kim[‡,*]

[†]Department of Bioengineering, Hanyang University, Seoul 133-791, Korea, [‡]Department of Chemistry, Pohang University of Science and Technology, Kyungbuk 790-784, Korea, [§]School of Chemical and Biological Engineering & Research Center for Energy Conversion and Storage, Seoul National University, Seoul 151-744, Korea, and [∥]Department of Materials Science & Engineering, Pohang University of Science and Technology, Kyungbuk 790-784, Korea. [¶]These authors contributed equally to this paper.

ABSTRACT A simple and novel electrostatic coupling method is reported, which provides a hyaluronic acid—quantum dot conjugate (HA—QD) that is colloidally stable and size-tunable from 50 to 120 nm. The HA—QDs show cancer targeting efficiency, which suggests diagnostic and imaging applications. The conjugates are also demonstrated for the fluorescence staining capability for lymphatic vessels *in vitro* and *in vivo*. Using the HA—QDs in a small animal model, lymphatic vessels are visualized real-time *in vivo* for days. Comprehensive cytotoxicity evaluations are made for the conjugates and the unconjugated counterpart. The HA—QDs showcase the potentials toward cancer imaging and real-time visualization of changes in lymphatic vessels such as lymphangiogenesis.

KEYWORDS: hyaluronic acid · fluorescence · lymphangiogenesis · quantum dots · surface modification

Semiconductor nanocrystal quantum dots (QDs) can be advantageous nanoemitters over conventional organic fluorophores for biological imaging.[1−3] QDs can have narrow and symmetric emission profiles that can be tuned from visible to infrared wavelengths. They are relatively more robust against photobleaching, which suites them for long-term imaging. They can be easily multiplexed by a single excitation source due to their broad absorption profiles. In order to exploit the advantages of QDs in *in vitro* or *in vivo* imaging, extensive studies have been made on QD−biomolecule conjugates such as QDs that are conjugated to antibody,[3−8] peptide,[9−12] aptamers,[13,14] and oligonucleotides.[15,16] The conjugations are typically made using small linker molecules,[3−7,9,11−14] polymers,[8] or avidin−biotin complex.[17] Small linker molecules can be advantageous in reducing the overall conjugate size. Smaller size is important not only for brighter signals per unit volume occupied by conjugates but also for better controls over the biodistributions or clearance pathways *in vivo*. Small linker conjugation typically involves carbodiimide-mediated peptide bond formation,[11] ester maleimide-mediated coupling,[10] or ester condensation. However, they often demand multistep procedures and may suffer from QD colloidal instabilities during the coupling reactions. Simple electrostatic coupling method is introduced for hyaluronic acid (HA)−QD conjugates. Conventionally, electrostatic couplings for QD conjugates use bridging macromolecules such as engineered recombinant proteins[5] or avidins.[6,7] Herein, we report a HA−QD conjugate (HA−QD) that is coupled by simple electrostatic interactions *via* a small linker molecule. They are colloidally stable and size-tunable from 50 to 120 nm and retain optical advantages of QDs.

HA, copolymers of *N*-acetyl D-glucosamine and D-glucuronic acid, is a nonsulfated glycosaminoglycan. It is one of the major components in the extracellular matrix that contributes significantly to cell proliferation and migration, wound healing, progression, metastasis, diagnosis, and prognosis of some malignant tumors.[18,19] For example, HA receptor CD44 overexpression is known to be strongly associated with cancerous angiogenesis and tumor progression.[20] Therefore, HA−QD can be a useful reporter probe that monitors tumor progressions, such as metastasis trafficking, or that screens anticancer drug efficacies.[21−24] HA−QD can be also used to visualize lymphatic vessels by fluorescence staining since HAs can be delivered into lymphatic endothelial cells through receptors such as lymphatic vessel endothelial receptor 1 (LYVE-1).[25,26] Lymphatic vessel

*Address correspondence to sungjee@postech.ac.kr, bskim@hanyang.ac.kr.

Received for review February 11, 2009 and accepted May 23, 2009.

Published online May 28, 2009.
10.1021/nn900138d CCC: $40.75

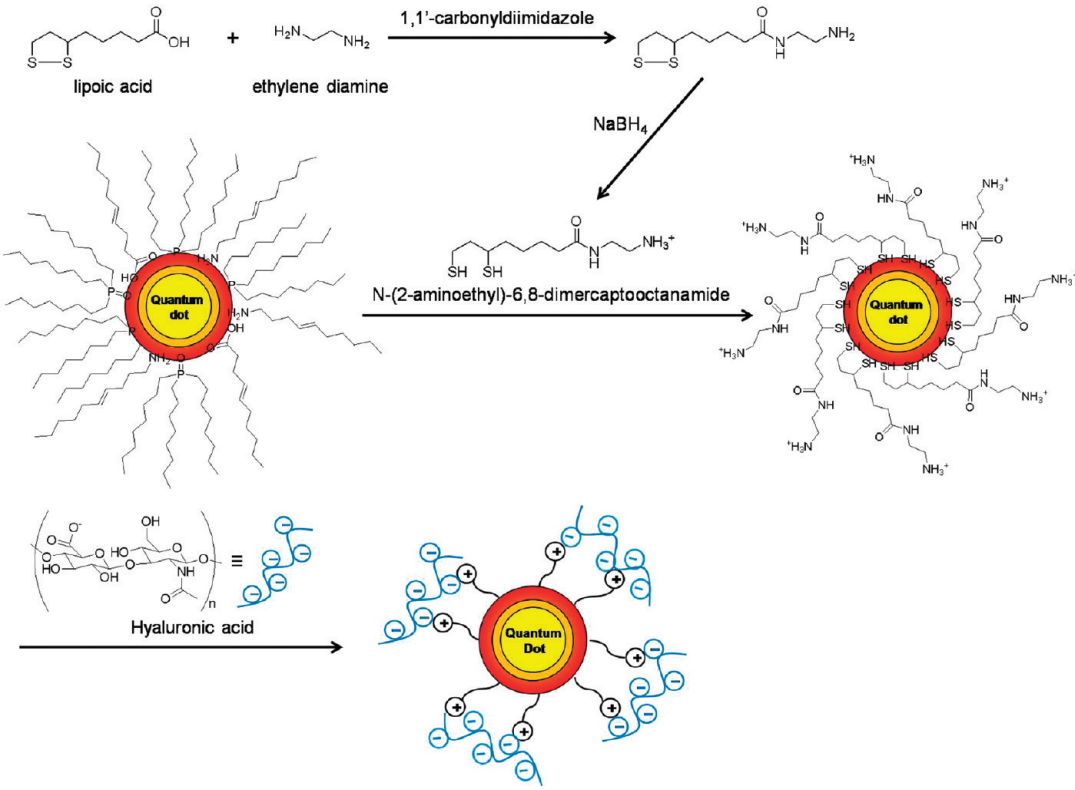

Scheme 1. Synthesis of hyaluronic acid−quantum dot conjugates.

staining by HA−QD can be especially advantageous for *in vivo* imaging since QDs can have strong fluorescence in near-infrared wavelengths that promise maximal tissue penetrations and minimal autofluorescence.[27] For example, they can be potentially used to real-time monitor the formation and development of lymphatic vessels around tumor mass such as lymphangiogenesis. Although QDs can be an ideal fluorescence probe for lymphatic vessel imaging, a large quantity of QD probes may be needed. Being an exogenous imaging contrast agent, any fluorescence probe needs large excess to overcome the limited cellular uptake and inherent signal diminution by cell proliferations. Compared to other targeting molecules, HA is extremely cost-effective and easily available in large quantity. Herein, we report that lymphatic vessels can be successfully visualized real-time *in vivo* for days using HA−QD.

RESULTS AND DISCUSSION

Multiple electrostatic adsorption is used to conjugate HA and QDs. HA has multiple negative charges. QDs can be positively modified by introducing a surface ligand (Scheme 1). The surface ligand is a small linker molecule that has dithiol for QD surface anchoring and primary amine for positive charge. As is shown in Scheme 1, it is synthesized by simple modification of lipoic acid with ethylene diamine followed by reductive disulfide cleavage reaction. The IUPAC name is *N*-(2-aminoethyl)-6,8-dimercaptooctanamide, and we name it amine-DHLA (meaning amine-containing dihydrolipoic acid derivative). CdSe/CdS/ZnS (core/shell/shell) QDs are prepared by similar procedures reported previously (see Experimental Methods).[28−31] The QDs are exposed to an excess amount of amine-DHLA for rigorous surface exchange (see Experimental Methods). After the surface ligand exchange, QDs become readily dispersible in aqueous media. The aqueous QDs show negligible changes in absorption and emission spectra when compared to as-prepared ones (see Supporting Information Figure S1).

The average hydrodynamic size is 8.4 nm in PBS buffer when measured by dynamic light scattering (DLS) method, and the ζ potential measures 27.1 mV in deionized water. The strongly positive charged surface enables individual dispersion of QDs. The average diameter of QDs measured by a transmission electron microscope (TEM) is 5.7 nm. HA of 3000 kDa molecular weight is used, which has approximately ~7500 carboxylic acid groups. The average hydrodynamic size of HA is 11.0 nm in PBS (10 nM). HA−QDs are prepared by mixing the positively charged QDs with HAs. Typical hydrodynamic size distributions of QD, HA, and HA−QD are shown in Figure 1a. When QDs are slowly added into HA PBS solution, hydrodynamic sizes of the resultant HA−QDs are measured (Figure 1b). The hydrodynamic size increases as the QD ratio increases. The conjugate shows 49.7 nm when the molar ratio of QD/HA is 1:10 and reaches 124 nm when the ratio becomes 4:1. The mixing molar ratio ranging between 1:10 and 4:1 of QD/HA produces conjugates of size from 50 to 120

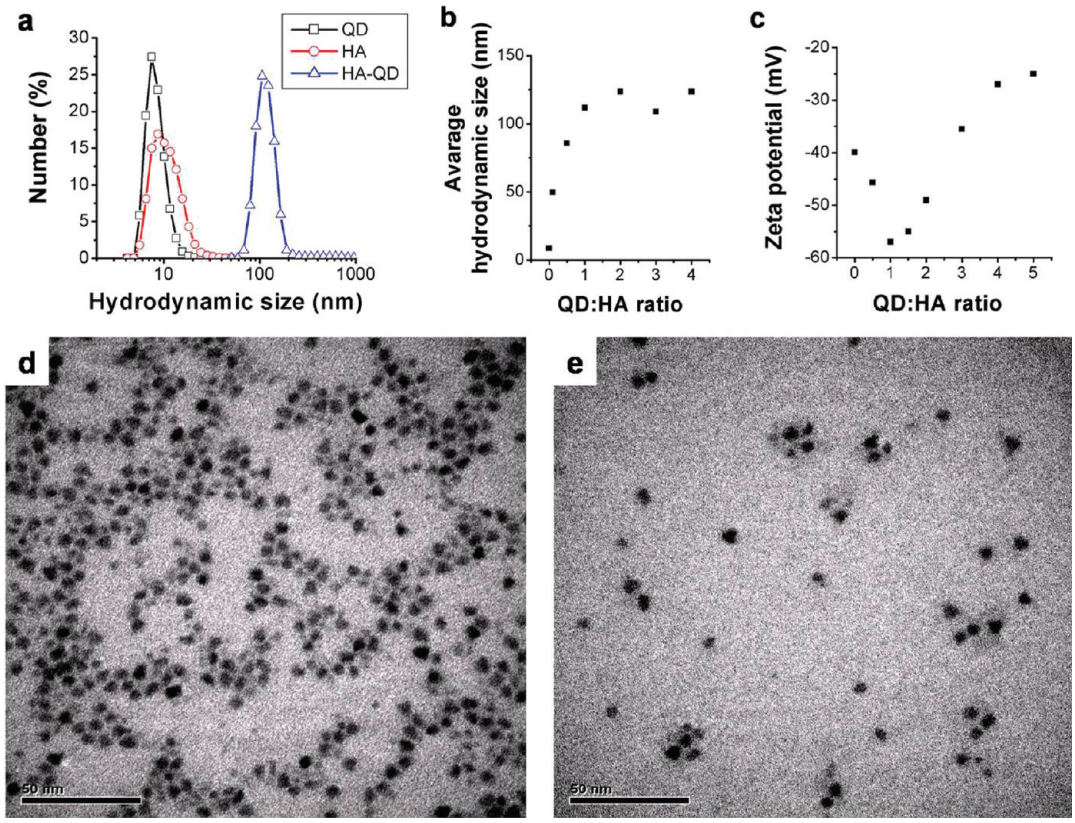

Figure 1. Hydrodynamic sizes of quantum dots (QDs), hyaluronic acids (HAs), and hyaluronic acid−quantum dot conjugates (HA−QD) in PBS buffer solutions measured by dynamic light scattering (a). Hydrodynamic size changes of HA−QDs with different ratio in PBS buffer (b). The ζ potential changes of HA−QDs with different ratios in deionized water (c). Transmission electron microscope images of QDs (d) and HA−QDs (e).

nm that are colloidally stable over weeks, showing no noticeable size increase or aggregations. When QD ratio exceeds 4:1, the conjugates start to aggregate and finally precipitate down from the solution. As shown in Figure 1c, absolute value of ζ potential decreases as the QD ratio increases and compensates the negative charges of HAs, which results in the colloidal instability. When HAs are in excess, absolute value of ζ potential increases as the QD ratio increases, presumably because they bind HAs close to each other. Individual electrostatic attraction between carboxylate in HA and amine on QD may not be as strong as a covalent bond; however, robust conjugation between HAs and QDs is made by multiple electrostatic bonds.

Mixing ratio of QD/HA for the conjugate shown in Figure 1a is 4:1. For *in vitro* and *in vivo* experiments herein, HA−QDs are made using 1:1 to 4:1 QD/HA mixing ratio. HA is larger than QD in hydrodynamic size and has larger amounts of charges. Thus HA can accommodate more than one QD but not *vice versa*. Slight excess of QD is chosen to minimize unconjugated HAs or QDs. Figure 1d,e shows TEM images of the QDs and HA−QDs that are used for Figure 1a. HA−QDs consist of one or multiple QDs, as is expected from the mixing ratio. HAs are relatively well visualized when bridged among QD clusters. In the case of conjugates with a single QD, HAs may stretch around the QD surfaces and make them hard to be visualized. HAs around QDs are further confirmed by uranyl acetate staining experiments (see Supporting Information Figure S2). No large aggregates are found under TEM, confirming our DLS data.

We use HeLa cells as a representative cancer cell that overexpresses HA receptors and human dermal fibroblast cell as a negative control. HeLa cells, human dermal fibroblast cells, and HeLa cells cultured with human dermal fibroblast cells are prepared. To visualize LYVE-1 expression, monoclonal LYVE-1 antibodies and FITC-conjugated secondary antibodies are used. The slides are mounted with 4,6-diamidino-2-phenylindole (DAPI) to blue stain nuclei and photographed using a confocal microscope (Figure 2a, see Experimental Methods). Immunocytochemistry results show that LYVE-1 is highly expressed in HeLa cells. Human dermal fibroblast cells are stained identically, but LYVE-1 expression is not detected. High contrast on LYVE-1 expression levels between HeLa cells and human dermal fibroblast cells is further manifested by staining co-cultured samples. To distinguish the human dermal fibroblast cells from HeLa cells when they are co-cultured, the cytoplasmic membranes of human dermal fibroblast cells are prelabeled with red DiI fluorescent probes. Both types of cells are stained simultaneously by DAPI and fluorescent LYVE-1 antibodies. Green fluorescence from

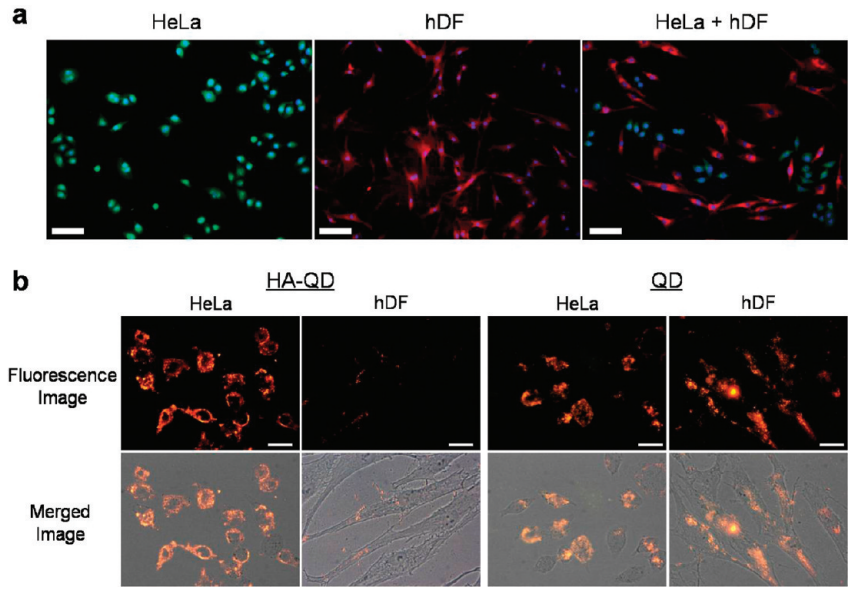

Figure 2. (a) Fluorescence microscope images of HeLa cells, human dermal fibroblast (hDF) cells, and co-cultured HeLa cells and hDF cells (fibroblast cells are prelabeled with DiI (red), LYVE-1 (green), and nuclei with DAPI (blue), respectively). (b) Hyaluronic acid−quantum dot conjugate (HA−QD) and quantum dot (QD) signals from HeLa cells and hDF cells. After the treatment of 100 nM of HA−QDs (ratio of QD/HA is 1:1) and QDs to HeLa cells and hDF cells for 2 h, the fluorescence images and merged images of fluorescence and transmission images are taken by optical microscope (figures are taken at ×400 magnification).

LYVE-1 staining can be only found around HeLa cell membranes.

Binding specificities of HA−QDs over unconjugated QDs are investigated with fluorescence microscopy. The HA−QDs are prepared by mixing HA and QD by a 1:1 ratio. Identical QDs that have amine-DHLAs are used for the mixing and for the unconjugated control sample. For LYVE-1 positive and negative cell lines, we use the previously confirmed HeLa cells and human dermal fibroblast cells; 100 nM of HA−QDs and unconjugated QDs are treated. Two hours after treatment, signals from QDs and HA−QDs are measured (Figure 2b). Specific bindings of HA−QDs into HeLa cells over human dermal fibroblast cells are observed. Strong QD signals from HA−QDs are found on HeLa cells. The HA−QDs are thought to effectively target the LYVE-1 on HeLa cells and subsequently internalize themselves in cytoplasm regions *via* receptor-mediated endocytosis. In contrast, QD signals from HA−QDs can be hardly found in human dermal fibroblast cells. In the case of unconjugated QDs, we find strong nonspecific bindings regardless of the cell type. Unconjugated QDs are unmistakenly found in both HeLa cells and human dermal fibroblast cells. Highly positive nature of the QD surface is ascribed to induce the nonspecific bindings. We stress that HA−QDs show selective targeting on LYVE-1 with negligible nonspecific bindings.

Cell-type-specific binding efficiencies of HA−QDs and unconjugated QDs are quantified by inductively coupled plasma atomic emission spectrometry (ICP-AES) (see Supporting Information Figure S3). The ICP-AES data represent the amounts of HA−QDs and QDs that are not bound to the cells and remained in cell culture media (see Experimental Methods). From that ICP-AES result, we can conclude that the amount of HA−QDs bound to HeLa cells is approximately four times larger than the amount of HA−QDs bound to the human dermal fibroblast cells. However, the amounts of unconjugated QDs bound to HeLa cells and human dermal fibroblast cells do not show noticeable difference.

We have demonstrated that HA−QDs can selectively fluorescence label cancerous cells that overexpress HA receptors. LYVE-1 is also a surface-bound HA receptor that is preferentially expressed by lymphatic endothelial cells (LEC). HA−QD can be used as a LEC trafficking agent and may allow us to follow LECs at the cellular level. Potentially, this can open a new window monitoring tumor growth and development real-time *in vivo*. However, before HA−QDs can be actively used for *in vivo* imaging, comprehensive cytotoxicity studies are required. Due to the unavoidable signal diminution as an exogenous imaging contrast agent, QD probes may demand high concentrations to label the targeted cells or tissues. Minimal cytotoxicity of HA−QDs is essential for *in vitro* and *in vivo* labeling applications. To determine the cytotoxicity of HA−QDs, HeLa cells and human dermal fibroblast cells are treated with 100 nM of HA−QDs and unconjugated QDs. Thirty minutes, 2 h, and 1 day after the treatment, 3-(4,5-dimethylthiazol-2-yl)-2,5-diphenyltetrazolium bromide (MTT) assay (Figure 3a), 3-amino-7-dimethylamino-2-methylphenazine hydrochloride (neutral red) assay (Figure 3b), and terminal uridine nick end labeling (TUNEL) assay are performed (Figure 3c,d). For mitochondrial metabolic activity evaluation, MTT assay is performed (see Experimental Methods). The HeLa cells and human dermal fibroblast cells treated with HA−QDs show higher mitochondrial metabolic activities compared to those of unconjugated QD-treated groups. Cell viability is evaluated by a rapid colorimetric test based on the uptake of a cationic supravital dye, neutral red, into the viable cells (see Experimental Methods). Neutral red assay also shows similar tendency that HeLa cells and human dermal fibroblast cells treated with HA−QDs have higher cell viability compared to QD-treated groups. However, HeLa cells and human dermal fibroblast cells treated with QDs or HA−QDs show decreased mitochondrial metabolic activity and cell viability compared to negative controls (cell without any QD or HA−QD treatment) at the same time points. It is noted that no significant level of cytotoxicity difference is observed

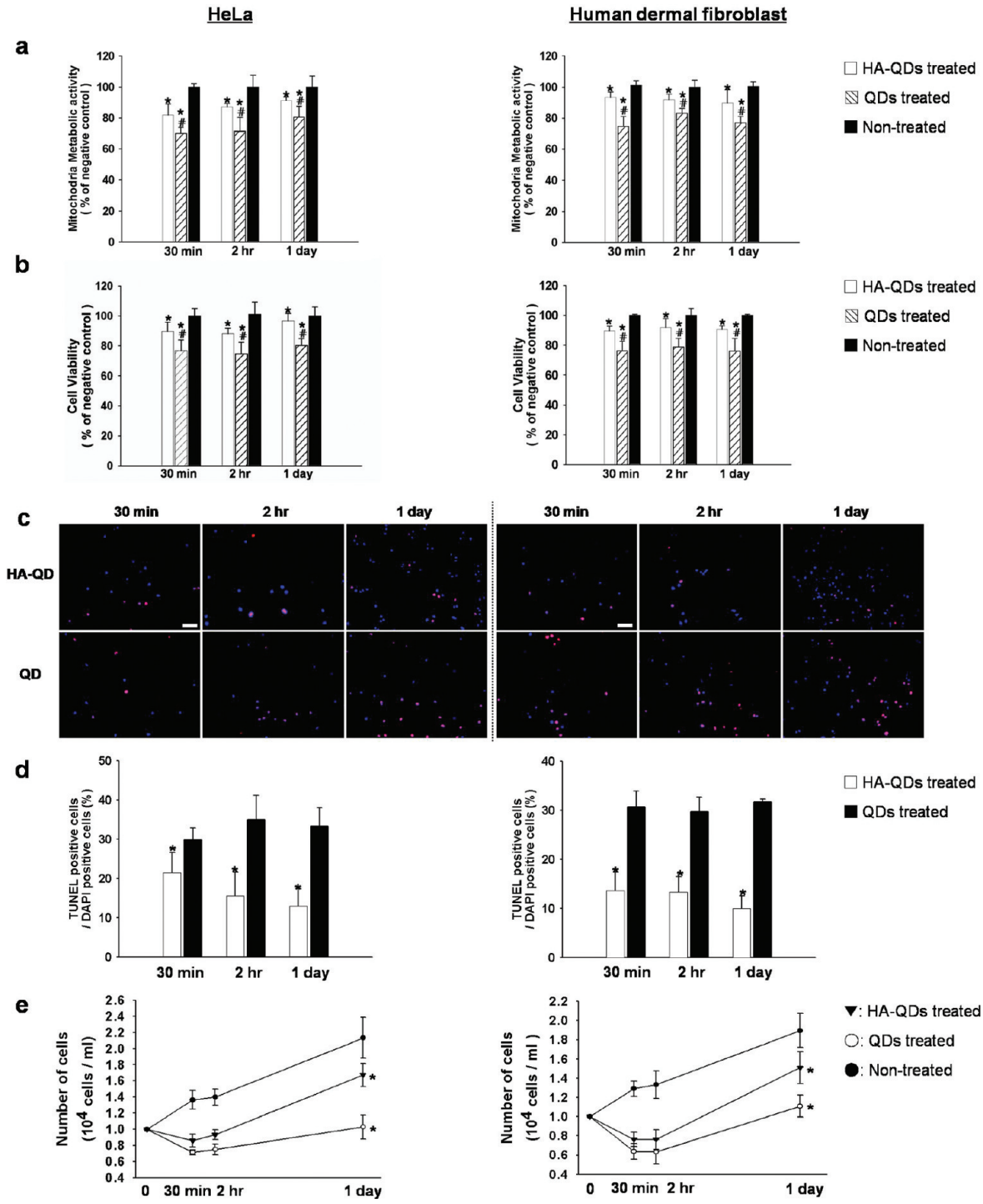

Figure 3. Cytotoxicity measurements of HeLa cells and human dermal fibroblast cells. Before the measurement, cells are treated with 100 nM of hyaluronic acid−quantum dot conjugates (HA−QDs, ratio of QD/HA is 1:1) and quantum dots (QDs) for 30 min, 2 h, and 1 day. (a) Mitochondrial metabolic activity determined by MTT assay, (b) cell viability determined by neutral red assay (negative control: cells without QD or HA−QD treatment, *$p < 0.05$ compared to negative control; #$p < 0.05$ compared to the HA−QD-treated groups), (c) apoptotic activity by TUNEL assay, (d) quantitative results of (c) (*$p < 0.05$ compared to QD-treated groups), (e) cell proliferation results.

for the different cell types, though HeLa cells uptake as much as 4 times more HA−QDs than human dermal fibroblast cells. TUNEL assay is performed to determine the apoptotic activity of HeLa cells and human dermal fibroblast cells treated with HA−QDs or unconjugated QDs. ApopTag Red *in situ* apoptosis detection kit (Chemicon, Temecula, CA) and DAPI are used to stain the apoptotic cell or cell fragment and nuclei of cells (Figure 3c). Compared to the HA−QD-treated cells, cells treated with QD show dramatically enhanced apoptotic activity. More than 30% of HeLa cells and human dermal fibroblast cells treated with QDs show apoptotic

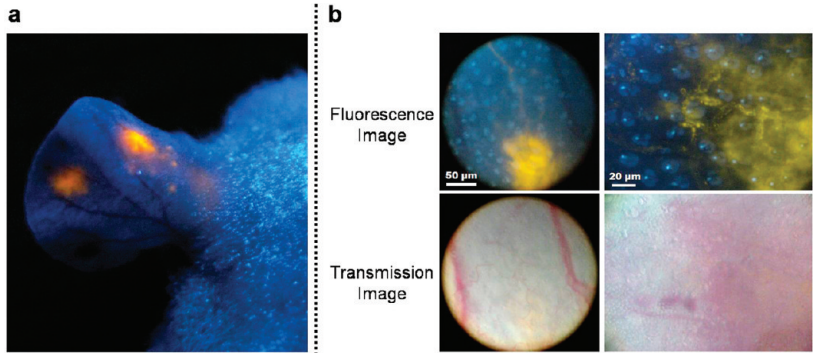

Figure 4. (a) Image of a mouse ear taken under UV lamp; 200 nM of hyaluronic acid−quantum dot conjugate solutions (ratio of QD/HA is 4:1) is injected subcutaneously at two different sites that are glowing in the image. (b) Fluorescence (top row) and transmission (bottom row) microscope images of a hyaluronic acid−quantum dot conjugate injection site at low (left column) and high (right column) magnifications. The microscope images are taken within 30 min after the injection.

activity. Apoptotic activity of HeLa cells and human dermal fibroblast cells treated with HA−QDs is significantly low: 13 and 9% of total cells, respectively, until 1 day. The MTT assay, neutral red assay, and TUNEL assay results show accordance tendency. HA conjugation to QD reduces the cytotoxicity for more than 24 h. HeLa cells and human dermal fibroblast cells treated with HA−QDs showed significantly decreased cytotoxicity compared to unconjugated QD-treated cells. The reinforced cytotoxicity shown in unconjugated QD-treated groups might have been caused by the membrane-disruptive interactions that occur in the highly positive surfaces. After treating HA−QDs or unconjugated QDs to HeLa cells and human dermal fibroblast cells, the cell proliferation differences are compared (Figure 3e). The initial cell density of HeLa cells and human dermal fibroblast cells are 1×10^4 cells/mL and cultured for 24 h after treating with HA−QDs or unconjugated QDs. HA−QD-treated cells show comparable cell proliferation results compared to those of unconjugated QD-treated groups. The cells treated with HA−QDs show minimal initial cytotoxicity for a few hours; however, cells treated with unconjugated QDs showed up to 40% of cells death within a few hours. Cytotoxicities of QDs or QD conjugates have been actively studied.[32−36] Cytotoxicity of QD conjugates depends on the nature of protecting inorganic shell layers (presumably related to the heavy metal ion leakage), sign of the conjugate surface charge, and distribution of the charges. Our CdSe/CdS/ZnS core/shell/shell QDs have well-passivated double-shell protecting layers with gradient crystal lattice mismatches from CdSe, CdS, and to ZnS. The reduced crystal lattice mismatches are thought to form well-passivating inorganic shell layers with fewer defects. Our CdSe/CdS/ZnS core/shell/shell QDs show lower cytotoxicity than CdSe QDs or CdSe/ZnS core/shell QDs in ref 34. We also speculate that the intrinsic biocompatibility of HA rendered the HA−QD conjugates to be less toxic.

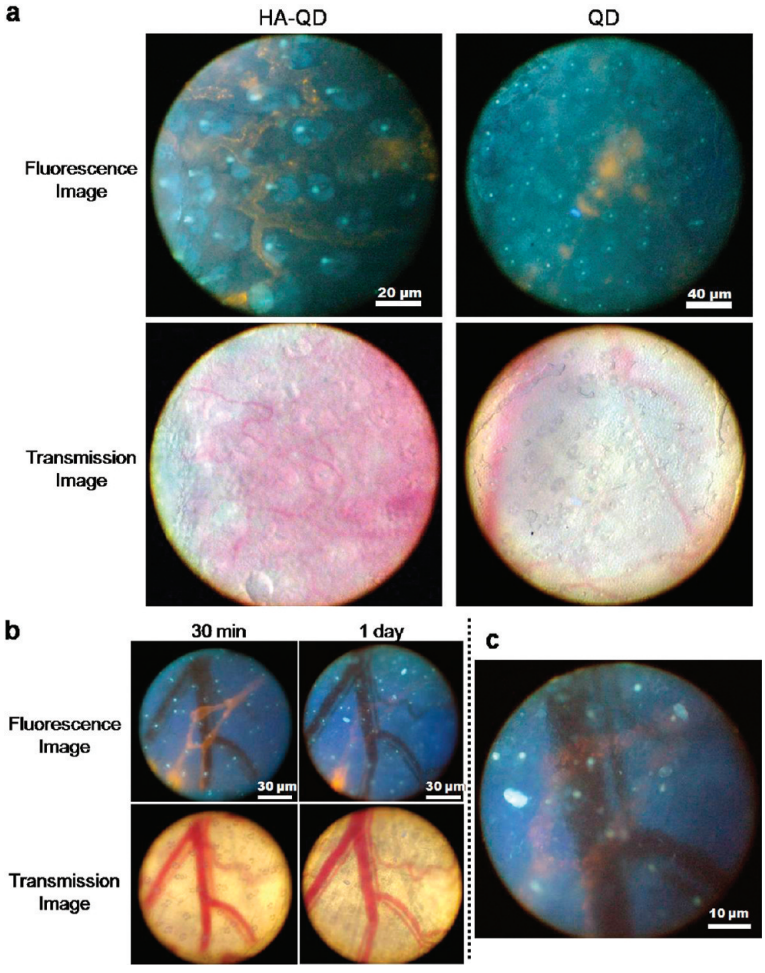

Figure 5. (a) Fluorescence (top row) and transmission (bottom row) microscope images near the subcutaneous injection sites of 200 nM of hyaluronic acid−quantum dot conjugate (HA−QD, ratio of QD/HA is 4:1) solution (left column) and unconjugated quantum dot (QD) solution (right column). Images are taken 30 min after the concurrent injections. (b) Fluorescence (top row) and transmission (bottom row) microscope images near a subcutaneous HA−QD injection site. Images are taken 30 min (left column) and 1 day (right column) after the injection. (c) Enlarged fluorescence image taken 1 day after injection.

Since we have confirmed the specific labeling ability of HA−QDs for LYVE-1 expressing cell lines with low cytotoxicity, HA−QDs are further applied for *in vivo* lymphatic vessel imaging; 100 μL of 200 nM HA−QD and unconjugated QD PBS solutions are each injected subcutaneously to ears of nude mice. The ratio between QD and HA is chosen to be 4:1. The average size and the size distribution are measured by dynamic light scattering (see Supporting Information Figure S4). The average size measures 58 nm. Lymphatic nanoparticle

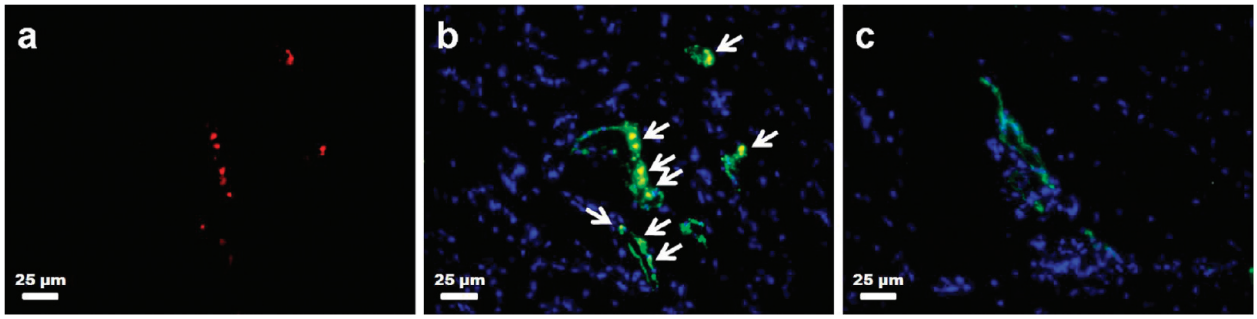

Figure 6. Fluorescence microscope images of mouse ear tissues near the hyaluronic acid−quantum dot conjugate (HA−QD) injection site (a,b) and near the unconjugated QD injection site (c). The mouse ear tissues are vertically sectioned at 30 min after the subcutaneous injection of 200 nM HA−QD or unconjugated QD solution. The tissues are stained simultaneously by DAPI and fluorescent LYVE-1 antibodies. (a) Filter set is chosen to selectively show red fluorescence from QDs. (b,c) Fluorescence images are merged to overlay the red (QD), green (LYVE-1), and blue (DAPI) signals. The bright yellow co-localization spots of QD and LYVE-1 signals are indicated by arrowheads in (b).

transportation is heavily governed by the size.[37,38] The smaller nanoparticles show the more efficient transportation, and the efficiency drops as the particle size increases. For example, 100 nm size polymer nanoparticles show ~10% lymph node targeting efficiency through lymphatic capillaries and vessels when compared to 25 nm size nanoparticles.[38] We judiciously choose ~60 nm average size HA−QDs since they show moderately efficient lymphatic flow transportations from the subcutaneous injection site. In addition, our HA−QDs are expected to have small diffusion coefficients due to the relatively large size. The slow lymphatic flow maximizes the retention time of our HA−QDs in lymphatic vessels to bind LECs. Typical injection sites are visualized under UV lamp in Figure 4a. We observe the injection sites using an inverted fluorescence microscope (Carl Zeiss, Axiovert 40 CFL). Fluorescence mode is used to visualize QD signals, and transmission mode shows the skin and blood vessels. As are shown in Figure 4b, the injection sites are glowing by the HA−QD fluorescence. The injected solutions are rapidly taken into the lymphatic drainage within a few minutes and begin to reveal the lymphatic vessels around the injection sites. In Figure 5, we compare the lymphatic vessel visualizations made by HA−QDs and by unconjugated QDs. Both injections are made concurrently, and the images are taken 30 min after the injections (Figure 5a). In the case of HA−QDs, we observe crisp visualization of lymphatic vessels with bright fluorescence along the inner walls of the vessels. In contrast, unconjugated QDs visualize the vessels in a faint and blurred fashion. As expected, specific binding of HA−QDs to the LECs in lymphatic vessels may have resulted in the bright fluorescence visualization. However, considering the short elapsed time after injection, larger hydrodynamic size of HA−QDs over unconjugated QDs, thus enhanced retention time around the injection site, may also contribute to the visualization contrast. We verify the labeling ability of the HA−QDs to lymphatic vessels by long-term monitoring of the QD signals (Figure 5b). We are able to follow a specific imaging spot using unique blood vessel patterns as a locational marker (see Supporting Information movie). We find that the fluorescence visualization of lymphatic vessels by HA−QDs lasts days (see Supporting Information Figure S5). We assume that the QD visualization signal reduction over time results from desorption of nonspecifically bound conjugates from the inner walls of the lymphatic vessels as well as the clearance of the conjugates in the lymphatic flow. It is also possible that QD fluorescence efficiency decreases as the HA−QDs are uptaken into the LECs. However, this may not be a major reason considering the fact that we do not observe noticeable QD fluorescence quenching as the HA−QDs are internalized into LECs *in vitro*. On the other hand, we are not able to find any detectable QD signals on lymphatic vessels only a few hours after injection when same amount of unconjugated QDs is delivered by identical method. To further confirm if HA−QDs can cell-specifically label lymphatic vessels *in vivo* tissue sectioning studies are carried out using the actual lymphatic vessels (see Experimental Methods). To determine whether the HA−QDs are indeed bound or internalized to lymphatic endothelial cells *in vivo*, the mouse ear tissues are immunofluorescently stained after injection of HA−QD and unconjugated QD solutions. HA−QD and unconjugated QD PBS solutions are concurrently injected by the identical method described for Figures 4 and 5. For both cases, mouse ear tissues around the injection sites are vertically sectioned at 30 min after the subcutaneous injection of HA−QD or unconjugated QD solution. The tissues are stained simultaneously by DAPI and fluorescent LYVE-1 antibodies. Lymphatic endothelial cells are detected by LYVE-1 antibodies and FITC-conjugated secondary antibodies. Figure 6a,b shows fluorescence microscope images of mouse ear tissues near the HA−QD injection site, and Figure 6c is near the unconjugated QD injection site. For Figure 6a, the fluorescence filter set is chosen to selectively show red fluorescence from QDs. Figure 6b,c shows merged images of the three fluorescence images by different filter sets

each for red-fluorescent QD, green-fluorescent LYVE-1 antibodies, and blue-fluorescent DAPI. In the case of HA−QD injection, bright yellow co-localization spots of QD and LYVE-1 signals are found, as indicated by arrowheads in Figure 6b. On the other hand, no co-localization can be found for unconjugated QD injection. The co-localization demonstrates the LYVE-1 specificity of HA−QDs *in vivo*, in addition to their specificity *in vitro* as shown in Figure 2. HA−QDs bind and/or internalize *in vivo* to LECs *via* the LYVE-1 specificity. In the case of unconjugated QD injection, no detectable QD can be found for the sectioned tissue samples. In Figure 6c, only FITC-stained lymphatic tissues can be found with DAPI signals.

Due to the constant lymphatic flow, the actual amount of HA−QDs which is uptaken by LECs and that acts as lymphatic vessel imaging contrast agents may be relatively small when compared to the administered amount. Therefore, multiple injections may be required around a region where the lymphatic vessels are desired to be vividly visualized. Currently, we pursue this to visualize the lymphatic vessel development and growth *in vivo* around tumor mass in a small animal model. QDs that emit longer wavelength (*i.e.*, near-infrared) are tried to guarantee the maximal tissue penetrations. On the basis of the studies reported herein, we believe HA−QDs can help visualize tumor progressions real-time *in vivo* by trafficking LECs in lymphatic vessels for extended time.

CONCLUSIONS

We have successfully made HA−QDs by using simple electrostatic attractions between HA and QD. A simple linker molecule is designed positively charged and used to form secure multiple electrostatic bonds for the conjugates. The HA−QDs are colloidally stable and flexibly size-tunable. HA−QDs specifically bind to HeLa cells when HeLa cells are used as a representative cancer cell that overexpresses HA receptors and human dermal fibroblast cell as a negative control. This suggests potential applications of HA−QDs for cancer imaging. Comprehensive cytotoxicity investigations are made for HA−QDs, especially relative to the unconjugated QDs, using cell viability, mitochondrial metabolic activity assay, apoptotic activity assay, and cell proliferation assay. The HA−QDs show remarkably low cytotoxicity, which suits them well for *in vivo* applications. Since the HeLa cells are confirmed expressing LYVE-1, HA−QDs are further applied for *in vivo* lymphatic imaging. Using a small animal model, we successfully label the lymphatic vessels *in vivo* by endocytosis-mediated HA−QD-stained LECs. We are able to clearly visualize the lymphatic vessels *in vivo* for up to days. We believe that the simple QD conjugate model herein can open a new door to development of real-time *in vivo* QD imaging that may have great potentials including tumor mechanism studies and anticancer drug screenings.

EXPERIMENTAL METHODS

Materials. Oleic acid (tech, 90%), trioctylphosphine (tech, 90%, TOP), 1-octadecene (tech, 90%, ODE), oleylamine (tech, 70%), diethylzinc, bis(trimethylsilyl)sulfide (95%), 1,1′-carbonyldiimidazole (CDI), and (±)-α-lipoic acid were purchased from Aldrich. Cadmium acetate dehydrates (99.999%) and selenium shots (99.99%) were purchased from Alfa Aesar and Strem, respectively. Ethylene diamine and sodium borohydride (99%) were purchased from Sigma-Aldrich.

Synthesis of CdSe/CdS/ZnS Core/Shell/Shell Quantum Dots. CdSe bare nanocrystals are made by the following procedure. For cadmium precursor, cadmium acetate (1.2 mmol) is dissolved in oleic acid (6.0 mmol) at 100 °C under vacuum. After the solution has cooled to room temperature, the cadmium precursor is mixed with selenium precursor. The selenium precursor is previously prepared by dissolving selenium shots (6.0 mmol) in TOP (6 mL) in a glovebox. ODE (40 mL) and oleylamine (6 mmol) are loaded into a three-neck flask and heated to 300 °C under nitrogen gas flow. At this temperature, the mixture of cadmium and selenium precursors is quickly injected into the reaction flask and the temperature is maintained at 280 °C. The reaction mixture is kept stirred until desired size of CdSe nanocrystals is obtained. Upon completion, the mixture is cooled to room temperature and diluted by hexanes. For purification, the product mixture is precipitated by excess methanol, collected by centrifugation, and redispersed to a small amount of hexanes.

CdS and ZnS shells are deposited onto CdSe bare nanocrystals by the following procedure. For cadmium precursor, cadmium acetate (0.3 mmol) is dissolved in oleic acid (1.5 mmol) at 100 °C under vacuum. When the solution has cooled to room temperature, the cadmium precursor is mixed with sulfide precursor. The sulfide precursor is previously prepared by dissolving bis(trimethylsilyl)sulfide (45 μL) in TOP (3 mL) in a glovebox. For precursor of zinc and sulfide, diethylzinc (130 μL) and bis(trimethylsilyl)sulfide (240 μL) are dissolved to TOP (5 mL). ODE (45 mL) is loaded into a four-neck flask. Under nitrogen gas flow, CdSe bare nanocrystals (9.0×10^{-4} mmol) are placed in the reaction flask. When the temperature of the reaction flask reaches 120 °C, the mixture of Cd and S precursors is slowly added using a syringe pump. After 30 min for the CdS shell growth, the temperature is raised up to 140 °C followed by dropwise addition of the mixture of Zn and S precursors. The temperature is maintained for 30 min for the ZnS shell growth. The final product of CdSe/CdS/ZnS (core/shell/shell) QD is purified by a similar method described above.

Surface Modification of CdSe/CdS/ZnS Core/Shell/Shell Quantum Dots with Amine-DHLA Surface Ligands. Precursor of amine-DHLA is made by CDI coupling of lipoic acid with ethylene diamine. (±)-α-Lipoic acid (20 mmol) and CDI (26 mmol) are dissolved in anhydrous chloroform (30 mL) and stirred under N_2 flow for 20 min at room temperature. The solution is added dropwise to ethylene diamine (100 mmol) in an ice bath and stirred for 2 h under N_2 gas flow. The crude product is washed three times by 10% NaCl aqueous solution (80 mL) and twice by 10 mM NaOH aqueous solution (80 mL). It is dried with magnesium sulfate, and the solvent is removed using a rotary evaporator to obtain yellow liquid (4.0 g). Reaction yield of the precursor is 80.5%.

CdSe/CdS/ZnS (core/shell/shell) QDs are ligand exchanged with amine-DHLAs for the conjugation with hyaluronic acid (HA). Excess amount (typically more than million times the number of QDs) of the precursor of amine-DHLA is dissolved in mixed solvent of $CHCl_3$ and MeOH (1:2, vol/vol, 3 mL). Two equimolar amounts of sodium borohydride is added to the solution and vigorously stirred for 20 min under N_2 gas flow at room temperature. Chloroform QD solution (1 mL) is added to the solution and further stirred for 20 h at room temperature. QDs are trans-

ferred to pH 3.7 acetate buffer aqueous layer by extraction. To remove excess free amine-DHLAs, the QD solution is dialyzed twice using Amicon 50 kDa M_W cutoff centrifugal filter.

Cell Culture Condition. HeLa cells, human dermal fibroblast cells, and HeLa cells cultured with human dermal fibroblast cells are maintained in Dulbecco's Modified Eagle's Medium (DMEM, Gibco BRL, Gaithersburg, MD) supplemented with 10% (v/v) fetal bovine serum (Gibco BRL) and 1% (w/v) penicillin/streptomycin (Gibco BRL) for cell adhesion. Cells are passaged every 5 days and used within 15 passages. For further test for cytotoxicity, cell proliferation and specific binding efficiency, cell culture medium is changed with DMEM medium with 1% (w/v) penicillin/streptomycin.

***In Vitro* Immunohistochemistry.** HeLa cells and human dermal fibroblast cells are fixed with 4% paraformaldehyde for 10 min at room temperature and washed with PBS. To visualize LYVE-1 expression, monoclonal antibodies against LYVE-1 are used. The samples are then incubated in deionized water containing FITC-conjugated secondary antibodies for 1 h at room temperature. The slides are mounted with 4,6-diamidino-2-phenylindole (DAPI, Vector Laboratories, Burlingame, CA) to stain nuclei and photographed using a confocal microscope. High contrast on LYVE-1 expression levels between HeLa cells and human dermal fibroblast cells is further manifested by staining co-cultured samples. To distinguish the human dermal fibroblast cells from HeLa cells when they are co-cultured, the cytoplasmic membranes of human dermal fibroblast cells are prelabeled with fluorescent probe Cell Tracker, 1,1′−1,1-dioactadecyl-3,3,3′,3′-tetramethylindocarbocyanine perchlorate (DiI, Invitrogen, Eugene, OR). Human dermal fibroblast cells are incubated in culture medium containing DiI dye (6.25 μg/mL) at room temperature for 2 h. The labeled cells are washed twice with PBS and cultured with HeLa cells. Both types of cells are stained simultaneously by DAPI and fluorescent LYVE-1 antibodies.

Quantification of Cell-Internalized QD Contents. Cell-type-specific binding efficiencies of HA−QDs and unconjugated QDs are quantified by inductively coupled plasma atomic emission spectrometry (ICP-AES, Shimadzu, Kyoto, Japan). The HeLa cells and human dermal fibroblast cells are treated with same amounts of HA−QDs or unconjugated QDs. The cell cultured media and PBS remnants used for washing are collected to quantitatively evaluate the amounts of QDs that are not bound to the cells. To the retrieved remnants is added hydrochloric acid to digest QDs. Cadmium ion concentration is measured by ICP-AES and is used to calculate QD contents.

Cytotoxicity Assays. To determine the cytotoxicity of HA−QD conjugates, HeLa cells and human dermal fibroblast cells are treated with unconjugated QDs and HA−QDs (100 nM). Thirty minutes, 2 h, and 1 day after unconjugated QD or HA−QD treatment, 3-(4,5-dimethylthiazol-2-yl)-2,5-diphenyltetrazolium bromide (MTT) assay, neutral red assay, and terminal uridine nick end labeling (TUNEL) assay are performed.

For MTT assay, MTT solution (2 mg/mL in PBS, Sigma) is added to 10% (v/v) of cell culture medium and incubated for 4 h at 37 °C, then replaced with DMSO (100 μL per well) to dissolve the formazan crystals. Culture plates are placed in a humidified atmosphere of 5% (v/v) CO_2 and 95% (v/v) air at 37 °C for 30 min with shaking before the absorbance at 570 nm is measured using a spectrophotometer. Results are expressed as a percentage of the absorbance of the positive control.

For neutral red assay, the medium containing neutral red (50 μg/mL, Sigma) is replenished, and the cells are incubated for an additional 3 h. After incubation, the solution is rapidly removed and acetic acid (1%, v/v)/ethanol (50%, v/v) (0.2 mL) is added to extract the dye. After 5 min incubation at room temperature, the absorbance at 540 nm is read. The intensity of the red color obtained is directly proportional to the number of viable cells. Results are expressed as percentage of the absorbance of the sample to the negative control.

***Ex Vivo* Immunohistochemistry.** Mouse ear tissues harvested 30 min after the injection of HA−QDs or unconjugated QDs are embedded in OCT compound (TISSUE-TEK 4583, Sakura Finetek USA Inc., Torrance, CA), frozen, and cut into 10 μm thick sections at −22 °C. To detect HA−QD or QD signals in lymphatic vessels, sections are immunofluorescently stained with monoclonal LYVE-1 antibodies (Fitzgerald, MA). The staining signal for LYVE-1 antibodies is visualized with FITC-conjugated secondary antibodies (Jackson ImmunoResearch Laboratories, West Grove, PA). The sections are counterstained with DAPI.

Acknowledgment. This work was supported by the Korea Science and Engineering Foundation (KOSEF) grant funded by the Korea government (MOST) (R01-2006-000-10647-0 (2005)), (R0A-2008-000-20114-0 (2008)) and a grant of the Korea Health 21 R&D Project, Ministry of Health & Welfare, Republic of Korea (A060660 and A050082).

Supporting Information Available: UV−vis and PL spectra of QDs and HA−QDs, negatively stained TEM image of HA−QDs, ICP-AES data on QD and HA−QD cell treatment experiment, and still shots and a movie clip of lymphatic vessel imaging using HA−QDs. This material is available free of charge *via* the Internet at http://pubs.acs.org.

REFERENCES AND NOTES

1. Bruchez, M., Jr.; Moronne, M.; Gin, P.; Weiss, S.; Alivisatos, A. P. Semiconductor Nanocrystals as Fluorescent Biological Labels. *Science* **1998**, *281*, 2013–2015.
2. Chan, W. C. W.; Nie, S. Quantum Dot Bioconjugates for Ultrasensitive Nonisotopic Detection. *Science* **1998**, *281*, 2016–2018.
3. Wu, X.; Liu, H.; Liu, J.; Haley, K. N.; Treadway, J. A.; Larson, J. P.; Ge, N.; Peale, F.; Bruchez, M. P. Immunofluorescent Labeling of Cancer Marker Her2 and Other Cellular Targets with Semiconductor Quantum Dots. *Nat. Biotechnol.* **2003**, *21*, 41–46.
4. Dahan, M.; Levi, S.; Luccardini, C.; Rostaing, P.; Riveau, B.; Triller, A. Diffusion Dynamics of Glycine Receptors Revealed by Single-Quantum Dot Tracking. *Science* **2003**, *302*, 442–445.
5. Mattoussi, H.; Mauro, J. M.; Goldman, E. R.; Anderson, G. P.; Sundar, V. C.; Mikulee, F. V.; Bawendi, M. G. Self-Assembly of CdSe−ZnS Quantum Dot Bioconjugates Using an Engineered Recombinant Protein. *J. Am. Chem. Soc.* **2000**, *122*, 12142–12150.
6. Goldman, E. R.; Balighian, E. D.; Mattoussi, H.; Kuno, M. K.; Mauro, J. M.; Tran, P. T.; Anderson, G. P. Avidin: A Natural Bridge for Quantum Dot−Antibody Conjugates. *J. Am. Chem. Soc.* **2002**, *124*, 6378–6382.
7. Jaiswal, J. K.; Mattoussi, H.; Mauro, J. M.; Simon, S. M. Long-Term Multiple Color Imaging of Live Cells Using Quantum Dot Bioconjugates. *Nat. Biotechnol.* **2003**, *21*, 47–51.
8. Gao, X.; Cui, Y.; Levenson, R. M.; Chung, L. W.; Nie, S. *In Vivo* Cancer Targeting and Imaging with Semiconductor Quantum Dots. *Nat. Biotechnol.* **2004**, *22*, 969–976.
9. Lagerholm, B. C.; Wang, M.; Ernst, L. A.; Ly, D. H.; Liu, H.; Bruchez, M. P.; Waggoner, A. S. Multicolor Coding of Cells with Cationic Peptide Coated Quantum Dots. *Nano Lett.* **2004**, *4*, 2019–2022.
10. Cai, W.; Shin, D.-W.; Chen, K.; Gheysens, O.; Cao, Q.; Wang, S. X.; Gambhir, S. S.; Chen, X. Peptide-Labeled Near-Infrared Quantum Dots for Imaging Tumor Vasculature in Living Subjects. *Nano Lett.* **2006**, *6*, 669–676.
11. Delehanty, J. B.; Medintz, I. L.; Pons, t.; Brunel, F. M.; Dawson, P. E.; Mattoussi, H. Self-Assembled Quantum Dot−Peptide Bioconjugates for Selective Intracellular Delivery. *Bioconjugate Chem.* **2006**, *17*, 920–927.
12. Xue, F. L.; Chen, J. Y.; Guo, J.; Wang, C. C.; Yang, W. L.; Wang, P. N.; Lu, D. R. Enhancement of Intracellular Delivery of CdTe Quantum Dots (QDs) to Living Cells by Tat Conjugation. *J. Fluoresc.* **2007**, *17*, 149–154.
13. Chen, X.-C.; Deng, Y.-L.; lin, Y.; Pang, D.-W.; Qing, H.; Qu, F.; Xie, H.-Y. Quantum-Dot-Labeled Aptamer Nanoprobes Specifically Targeting Glioma Cells. *Nanotechnology* **2008**, *19*, 1–6.
14. Levy, M.; Cater, S. F.; Ellington, A. D. Quantum-Dot Aptamer Beacons for the Detection of Proteins. *ChemBioChem* **2005**, *6*, 2163–2166.

15. Chan, P.; Yuen, T.; Ruf, F.; Gonzalez-Maeso, J.; Sealfon, S. C. Method for Multiplex Cellular Detection of mRNAs Using Quantum Dot Fluorescent *In Situ* Hybridization. *Nucleic Acids Res.* **2005**, *33*, 1–8.
16. Pathank, S.; Choi, S.-K.; Arnheim, N.; Thompson, M. E. Hydroxylated Quantum Dots as Luminescent Probes for *In Situ* Hybridization. *J. Am. Chem. Soc.* **2001**, *123*, 4103–4104.
17. Le Gac, S.; Vermes, I.; van den Berg, A. Quantum Dots Based Probes Conjugated to Annexin V for Photostable Apoptosis Detection and Imaging. *Nano Lett.* **2006**, *6*, 1863–1869.
18. Laurent, T. C.; Fraser, J. R. Hyaluronan. *FASEB J.* **1992**, *6*, 2397–2404.
19. Fraser, J. R.; Kimpton, W. G.; Laurent, T. C.; Cahill, R. N.; Vakakis, N. Uptake and Degradation of Hyaluronan in Lymphatic Tissue. *Biochem. J.* **1988**, *256*, 153–158.
20. Gunthert, U.; Hofmann, M.; Rudy, W.; Reber, S.; Zoller, M.; Haubmann, I.; Martzku, S.; Wenzel, A.; Ponta, H.; Herrlich, P. A New Variant of Glycoprotein CD44 Confers Metastatic Potential to Rat Carcinoma Cells. *Cell* **1991**, *65*, 13–24.
21. Stacker, S. A.; Achen, M. G.; Jussila, L.; Baldwin, M. E.; Alitalo, K. Lymphangiogenesis and Cancer Metastasis. *Nat. Rev. Cancer* **2002**, *2*, 573–583.
22. Padera, T. P.; Kadambi, A.; di Tomaso, E.; Carreira, C. M.; Brown, E. B.; Boucher, Y.; Choi, N. C.; Mathisen, D.; Wain, J.; Mark, E. J.; Munn, L. L.; Jain, R. K. Lymphatic Metastasis in the Absence of Functional Intratumor Lymphatics. *Science* **2002**, *296*, 1883–1886.
23. Saharinen, P.; Tammela, T.; Karkkainen, M. J.; Alitalo, K. Lymphatic Vasculature: Development, Molecular Regulation and Role in Tumor Metastasis and Inflammation. *Trends Immunol.* **2004**, *25*, 387–395.
24. Eichten, A.; Hyun, W. C.; Coussens, L. M. Distinctive Features of Angiogenesis and Lymphangiogenesis Determine Their Functionality during *De Novo* Tumor Development. *Cancer Res.* **2007**, *67*, 5211–5220.
25. Banerji, S.; Ni, J.; Wang, S. X.; Clasper, S.; Su, J.; Tammi, R.; Jones, M.; Jackson, D. G. SYVE-1, a New Homologue of the CD44 Glycoprotein, is a Lymph-Specific Receptor for Hyaluronan. *J. Cell Biol.* **1999**, *144*, 789–801.
26. Prevo, R.; Banerji, S.; Ferguson, D. J. P.; Clasper, S.; Jackson, D. G. Mouse LYVe-1 is an Endocytic Receptor for Hyaluronan in Lymphatic Endothelium. *J. Biol. Chem.* **2001**, *276*, 19420–19430.
27. Kim, S.; Lim, Y. T.; Soltesz, E. G.; De Grand, A. M.; Lee, J.; Nakayama, A.; Parker, J. A.; Mihaljevic, T.; Laurence, R. G.; Dor, D. M.; Cohn, L. H.; Bawendi, M. G.; Frangioni, J. V. Near-Infrared Fluorescent Type II Quantum Dots for Sentinel Lymph Node Mapping. *Nat. Biotechnol.* **2004**, *22*, 93–97.
28. Dabbousi, B. O.; Rodriguez-Viejo, J.; Mikulec, F. V.; Heine, J. R.; Mattoussi, H.; Ober, R.; Jensen, K. F.; Bawendi, M. G. (CdSe)ZnS Core−Shell Quantum Dots: Synthesis and Characterization of a Size Series of Highly Luminescent Nanocrystallites. *J. Phys. Chem. B* **1997**, *101*, 9463–9475.
29. Murray, C. B.; Norris, D. J.; Bawendi, M. G. Synthesis and Characterization of Nearly Monodisperse CdE (E = S, Se, Te) Semiconductor Nanocrystallities. *J. Am. Chem. Soc.* **1993**, *115*, 8706–8715.
30. Peng, X.; Schlamp, M. C.; Kadavanich, A. V.; Alivisatos, A. P. Epitaxial Growth of Highly Luminescent CdSe/CdS Core/Shell Nanocrystals with Photostability and Electronic Accessibility. *J. Am. Chem. Soc.* **1997**, *119*, 7019–7029.
31. Yu, W. W.; Peng, X. Formation of High-Quality CdSe and Other II−VI Semiconductor Nanocrystals in Noncoordinating Solvents: Tunable Reactivity of Monomers. *Angew. Chem., Int. Ed.* **2002**, *41*, 2368–2371.
32. Derfus, A. M.; Chan, W. C. W.; Bhatia, S. N. Probing the Cytotoxicity of Semiconductor Quantum Dots. *Nano Lett.* **2004**, *4*, 11–18.
33. Hoshino, A.; Fujioka, K.; Oku, T.; Suga, M.; Sasaki, Y. F.; Ohta, T.; Yasuhara, M.; Suzuki, K.; Yamamoto, K. Physicochemical Properties and Cellular Toxicity of Nanocrystal Quantum Dots Depend on Their Surface Modification. *Nano Lett.* **2004**, *4*, 2163–2169.
34. Kirchner, C.; Liedl, T.; Kudera, S.; Pellegrino, T.; Munoz Javier, A.; Gaub, H. E.; Stölzle, S.; Fertig, N.; Parak, W. J. Cytotoxicity of Colloidal CdSe and CdSe/ZnS Nanoparticles. *Nano Lett.* **2005**, *5*, 331–338.
35. Chang, E.; Thekkek, N.; Yu, W. W.; Colvin, V. L.; Drezek, R. Evaluation of Quantum Dot Cytotoxicity Based on Intracellular Uptake. *Small* **2006**, *2*, 1412–1417.
36. Cho, S. J.; Maysinger, D.; Jain, M.; Roder, B.; Hackbarth, S.; Winnik, F. M. Long-Term Exposure to CdTe Quantum Dots Causes Functional Impairments in Live Cells. *Langmuir* **2007**, *23*, 1974–1980.
37. Reddy, S. T.; Rehor, A.; Schmoekel, H. G.; Hubbell, J. A.; Swartz, M. A. *In Vivo* Targeting of Dendritic Cells in Lymph Nodes with Poly(propylene sulfide) Nanoparticles. *J. Controlled Release* **2006**, *112*, 26–34.
38. Reddy, S. T.; van der Vlies, A. J.; Simeoni, E.; Angeli, V.; Randolph, G. J.; O'Neil, C. P.; Lee, L. K.; Swartz, M. A.; Hubbell, J. A. Exploiting Lymphatic Transport and Complement Activation in Nanoparticle Vaccines. *Nat. Biotechnol.* **2007**, *25*, 1159–1164.